Back-Contacted Silicon Heterojunction Solar Cells With Efficiency >21%

Andrea Tomasi, Bertrand Paviet-Salomon, Damien Lachenal, Silvia Martin de Nicolas, Antoine Descoeudres, Jonas Geissbühler, Stefaan De Wolf, and Christophe Ballif

***Abstract*—We report on the fabrication of back-contacted silicon heterojunction solar cells with conversion efficiencies above 21%. Our process technology relies solely on simple and size-scalable patterning methods, with no high-temperature steps. Using *in situ* shadow masks, doped hydrogenated amorphous silicon layers are patterned into two interdigitated combs. Transparent conductive oxide and metal layers, forming the back electrodes, are patterned by hot melt inkjet printing. With this process, we obtain high short-circuit current densities close to 40 mA/cm^2 and open-circuit voltages exceeding 720 mV, leading to a conversion efficiency of 21.5%. However, moderate fill factor values limit our current device efficiencies. Unhindered carrier transport through both heterocontact layer stacks, as well as higher passivation quality over the minority carrier-injection range relevant for solar cell operation, are identified as key factors for improved fill factor values and device performance.**

***Index Terms*—Amorphous silicon, crystalline silicon (c-Si), heterojunctions, photovoltaic cells, solar cells.**

I. Introduction

SILICON heterojunction (SHJ) technology is of high interest for application in solar cells; it combines the use of crystalline silicon (c-Si) wafers as optically active absorbers with thin-film silicon deposition technology for device fabrication [1]. The excellent c-Si surface passivation properties of hydrogenated amorphous silicon (a-Si:H) enable high open-circuit voltages ($V_{\rm oc}$) over 700 mV, as well as excellent low temperature coefficients in finished devices. The promise of this technology was recently further substantiated by Panasonic, Osaka, Japan, which reported conversion efficiencies as high as 24.7%, within the highest ever reached for c-Si-based solar cells of practical size to date [2]. The high level of surface passivation and the fact that SHJ device fabrication avoids any high-temperature processes makes this technology also, particularly, suited for thin wafers [3].

The fill factor (*FF*) and short-circuit current density ($J_{\rm sc}$) values of SHJ devices are comparable with those of typical homojunction devices. Despite the fact that tunneling may play an important role in carrier transport, the *FF* in SHJ devices has been empirically shown not to suffer from any significant fundamental limitation [2], compared with best homojunction technologies as passivated emitter, rear locally diffused [4] and back-contacted [5] solar cells. However, standard two-side contacted front-emitter silicon heterojunction (Std-SHJ) solar cells are limited by parasitic absorption of light, either in the a-Si:H films or the transparent conductive oxide (TCO). These $J_{\rm sc}$ losses are linked to the short-wavelength response of SHJ devices [6]. In the long-wavelength part of the spectrum, well-engineered SHJ devices can outperform the best reported homojunction solar cells [7].

A straightforward step toward higher $J_{\rm sc}$ values and higher conversion efficiencies in SHJ devices consists of the back-contacted architecture, featuring both electron and hole collection contacts at the rear of the solar cell. This cell concept—which is industrially proven by SunPower, Union City, CA, USA, in the case of homojunction devices with conversion efficiencies of up to 24.2% [5]—has the advantage of eliminating front-electrode shadowing. Moreover, in the case of SHJ devices, it brings additional benefits by minimizing or even eliminating parasitic absorption. In back-contacted SHJ solar cells, a front TCO layer is no longer required and the front a-Si:H layers can be tuned, irrespective of their carrier transport properties, solely in regard to their transparency and passivation properties. Actually, substitution of the complete TCO/a-Si:H stack with wider bandgap passivating dielectrics for improved transparency becomes possible.

The potential of back-contacted architectures using SHJ contacts was recently convincingly pointed out by Panasonic, Osaka, Japan, reporting the world's highest energy conversion efficiency of 25.6% for c-Si-based solar cells under 1-sun illumination [8]. This record device exhibits an area of 143.7 cm^2 and demonstrates, in addition to the enormous potentiality of the technology, its scalability to devices of practical size. Based on this new exciting result, back-contacted SHJ is arguably the ultimate device architecture for single-junction silicon wafer-based solar cells. Similarly, another impressive result was recently

Manuscript received February 11, 2014; revised April 15, 2014; accepted April 22, 2014. Date of publication May 14, 2014; date of current version June 18, 2014. This work was supported by the Swiss Commission for Technology and Innovation under Grant 13348.1, by the Axpo Naturstrom Fonds, by the European Commission (FP7 Project HERCULES) under Grant 608498, by the Office Fédéral de L'énergie, and by the Fonds National Suisse Reequip Program under Grants 206021_139135 and 206021_133832.

A. Tomasi, B. Paviet-Salomon, S. M. de Nicolas, J. Geissbühler, S. De Wolf, and C. Ballif are with the Photovoltaics and Thin-Film Electronics Laboratory, Institute of Microengineering, Ecole Polytechnique Fédérale de Lausanne, 2000 Neuchâtel, Switzerland (e-mail: andrea.tomasi@epfl.ch, bertrand.paviet-salomon@epfl.ch, silvia.martin-de-nicolas@epfl.ch, jonas.geissbuehler@epfl.ch, stefaan.dewolf@epfl.ch, christophe.ballif@epfl.ch).

D. Lachenal is with Roth & Rau Research AG, 2068 Neuchâtel, Switzerland (e-mail: damien.lachenal@roth-rau.ch).

A. Descoeudres is with the PV-Center, Centre Suisse d' Electronique et de Microtechnique, 2000 Neuchâtel, Switzerland (e-mail: antoine.descoeudres@csem.ch).

Color versions of one or more of the figures in this paper are available online at http://ieeexplore.ieee.org.

Digital Object Identifier 10.1109/JPHOTOV.2014.2320586

reported by Sharp, Japan; its so-called rear heterojunction emitter plus antireflective passivation layers concept, using interdigitated back contacts, yielded a conversion efficiency of 24.7%, on a cell area <4 cm^2 [9]. Furthermore, a conversion efficiency of 20.5%, on a cell area of 221 cm^2, was reached by LG, Korea [10], again by means of an interdigitated back-contacted silicon heterojunction (IBC-SHJ) device. Always in the field of IBC-SHJ devices, Helmholtz-Zentrum Berlin, Germany, has reported a conversion efficiency of 20.2% [11], whereas several other groups have presented solar cells with conversion efficiencies in the range of 15–20% [12]–[15]. Back-contacted SHJ devices using alternative contacting schemes have been reported as well [16]–[18]. In this case, a maximum conversion efficiency of 17.1% [19], with a rear point-contact scheme, has been shown. It is worth mentioning that the use of *in situ* shadow masks to structure a-Si:H layers in back-contacted SHJ, as proposed in this study, is an approach previously demonstrated; however, so far, only relatively modest device performances were achieved [20]–[23].

The implementation of all back-contact architectures typically adds complexity to the overall fabrication process; indeed, it requires adequate patterning technologies and accurate alignment techniques. In this study, we aimed for the fabrication of high-efficiency IBC-SHJ devices via simple processing technologies and a minimal number of processing steps, comparable with those required for the fabrication of Std-SHJ devices. In the first part of this paper, we describe the cell design and the proposed fabrication technology. In the second part, we analyze the solar cell results that are achieved so far, as well as the factors limiting current solar cell efficiencies.

II. Experimental Details

A. Solar Cell Design and Fabrication Process

In this paper, IBC-SHJ solar cells with 9-cm^2 active cell area were fabricated on 250-μm-thick, n-type, 4-in float-zone (FZ) wafers, with a nominal resistivity of 3 Ω·cm.

Wafer texturing was performed in a potassium hydroxide solution. Following wet-chemical cleaning of the surfaces and a short dip in a diluted hydrofluoric solution, an intrinsic a-Si:H layer and a thin intrinsic/n-type a-Si:H layer stack were deposited on the backside and on the front side of the wafer, respectively. The n- and p-type a-Si:H combs on the backside, needed for, respectively, electron and hole collection, were fabricated via *in situ* shadow masks. All a-Si:H layers were deposited by plasma-enhanced chemical vapor deposition (PECVD); details can be found elsewhere [24]. For the back electrodes, a thick TCO/metal stack was deposited on the full back surface of the cell precursor via physical vapor deposition (PVD). For an antireflection coating on the front side, a hydrogenated amorphous silicon nitride (a-SiN:H) layer was deposited by PECVD at sufficiently low temperature (<200 °C) to avoid annealing-induced degradation of the a-Si:H layers [25]. The TCO/metal stack was then patterned into two interdigitated combs by hot melt inkjet printing of an etch resist that was well aligned with the p- and n-type regions underneath, followed by wet etching of the exposed areas. A final curing step, at a temperature below 200 °C, was performed in a belt furnace. The resulting cell architecture is represented in Fig. 1.

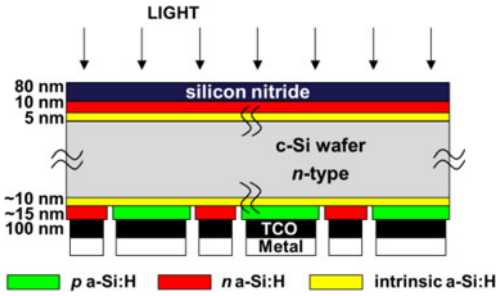

Fig. 1. Schematic of IBC-SHJ solar cell architecture.

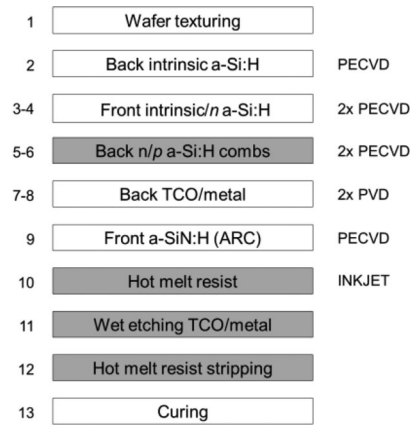

Fig. 2. Proposed IBC-SHJ process flow (patterning steps are highlighted with a gray background).

The overall cell fabrication process relies in total on six PECVD and two PVD steps, some of these without vacuum break, in the same reactor. Counting wafer texturing, hot melt inkjet printing, TCO/metal etching, hot melt stripping, and curing, we end up with only 13 processing steps for our IBC-SHJ processing sequence, to be compared with a total of ten steps required for typical Std-SHJ devices (wafer texturing, four PECVD, and three PVD layers plus metal-paste printing and curing). In Fig. 2, we show the overall process flow of our IBC-SHJ devices.

B. Patterning Techniques and Alignment Methodologies

The IBC-SHJ architecture requires patterning of the back n- and p-type a-Si:H layers and of the back TCO/metal stack. The patterning of the doped a-Si:H PECVD layers is critical due to the high-purity requirements of wafer surfaces during PECVD passivation processes and the need to strictly preserve the high quality of the intrinsic/p-type a-Si:H and intrinsic/n-type a-Si:H interfaces [26]. For patterning the doped a-Si:H PECVD layers, we laser cut masks from c-Si wafers. Alignment between the mask and substrate in the PECVD deposition chamber was achieved by means of an especially designed substrate holder and metal pins. The deposition rate of a-Si:H through 1-mm- (n-type a-Si:H) and 1.4-mm-wide (p-type a-Si:H) mask slits was found to be, respectively, 52% and 12% lower,

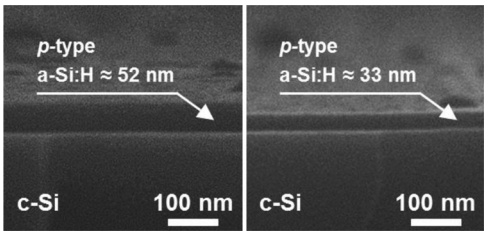

Fig. 3. SEM cross sections of a thick p-type a-Si:H layer on a polished silicon wafer, patterned via *in situ* masking, close to the center (left image) and edge (right image) of the deposited feature, respectively. The deposition rate through a 1.4-mm-wide mask slit is reduced by 12% compared with a full-area PECVD a-Si:H deposition.

compared with full-area PECVD a-Si:H deposition. The reduction of the a-Si:H deposition rate through a mask slit was confirmed by both ellipsometry and scanning electron microscope (SEM) cross-sectional observations. Moreover, SEM micrographs of a thick p-type a-Si:H layer, deposited on a polished silicon wafer through an *in situ* shadow mask, reveal tapering of the a-Si:H layer thickness toward the edge of the deposited feature (see Fig. 3). For patterning the TCO/metal stack, we used hot melt inkjet printing combined with wet etching, as already mentioned. Features as small as 50 μm can be easily achieved via hot melt inkjet printing, enabling the fabrication of IBC electrodes [27]. In our case, the alignment of the hot melt inkjet print over the patterned doped a-Si:H layers was achieved by fiducials laser-marked on the wafer.

We estimate an overall accuracy of ± 15 μm for the positioning of the TCO/metal combs over the mask-patterned a-Si:H layers. The main error sources are linked to laser distortion in marking and mask fabrication, and mask positioning during PECVD processes. In designing the hot melt inkjet etch resist, underetching effects were also considered for accurate patterning. To account for these positioning errors, the width of the TCO/metal comb fingers in our cells is kept narrower than that one of the doped a-Si:H comb fingers underneath. From optical microscopy images, we can evaluate that the TCO/metal electrodes cover the p- and n-type a-Si:H layers by $\sim$89% and $\sim$85%, respectively. However, these coverage fraction values, with respect to those reported in [21] and [28], are underestimated. The very edges of the doped a-Si:H comb fingers are indeed electronically inactive due to the observed thickness tapering effects. The alignment quality can be assessed from Fig. 4, where both a p-type a-Si:H layer and a TCO/metal electrode are visible, whereas an n-type a-Si:H layer is weakly visible.

III. Results and Discussion

A. Interdigitated Back-Contacted Silicon Heterojunction Solar Cell Results

The 1-sun current–voltage (*I–V*) characteristics of our IBC-SHJ solar cells were measured in-house under AM-1.5G at a temperature of 25 °C. The designated cell area of 9 cm^2 was defined by a shadow mask, excluding the busbar region at the rear. For the following discussion (see Sections III-A and B), we chose a representative 9-cm^2 IBC-SHJ device for which the

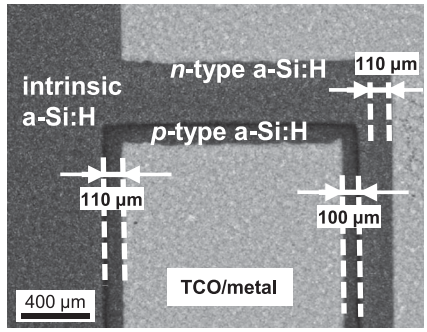

Fig. 4. Alignment quality of doped a-Si:H layers and TCO/metal electrode for use in our IBC-SHJ solar cells. In the area between the doped a-Si:H layers, the textured silicon surface is covered only by an intrinsic a-Si:H layer.

TABLE I
Electrical Parameters and FF Losses of IBC-SHJ (see Sections III-A and B), Best IBC-SHJ (see Sections III-C), and Best Std-SHJ Devices

Parameter	IBC-SHJ (Sections III.A and III.B)	Best Std-SHJ [29]	Best IBC-SHJ (Section III.C)
V_{oc} (V)	0.726	0.727	0.724
J_{sc} (mA/cm^2)	39.5	38.9	39.9
E*ff* (%)	20.9	22.1	21.5
FF (%)	73.0	78.4	74.5
R^N_{series} (Ω·cm^2)	2.1	1.1	1.3
ΔFF_R_{series} (%)	10.4	5.2	6.6
ΔFF_J(n≠1) (%)	1.6	1.4	3.8

a-Si:H layers, apart from the deposition time, were deposited with the same plasma conditions as in our best certified 4-cm^2 Std-SHJ device [29]. The chosen IBC-SHJ device shows a conversion efficiency of 20.9%, a $V_{\rm oc}$ of 726 mV, and a $J_{\rm sc}$ of 39.5 mA/cm^2. We compare these parameters with those of our best certified Std-SHJ device (see Table I). The achieved $V_{\rm oc}$ of 726 mV is only 1 mV lower than that of our best Std-SHJ device, demonstrating the compatibility of our IBC processing sequence with high-quality a-Si:H passivation layers. The measured $J_{\rm sc}$ of 39.5 mA/cm^2 is 0.6 mA/cm^2 higher than the $J_{\rm sc}$ of our silver-printed best certified Std-SHJ device. Conversely, the IBC-SHJ device *FF* is 73.0%, which is significantly lower than any typical high-performance Std-SHJ device. Based on spectral response and light-beam-induced current measurements, we link the still relatively modest $J_{\rm sc}$ gain in our IBC-SHJ devices (versus our best Std-SHJ device) to not fully minimized parasitic absorption losses (both in the short- and long-wavelength parts of the spectrum), rather than to electrical shading effects [30], [31]. Further details on this topic will be the subject of future research.

B. Fill-Factor Losses: Interdigitated Back-Contacted Silicon Heterojunction and Best Standard Two-Side Contacted Front-Emitter Silicon Heterojunction Solar Cells

Deviation of the *FF* of a solar cell from its ideal value is generally the result of loss mechanisms related to charge–carrier

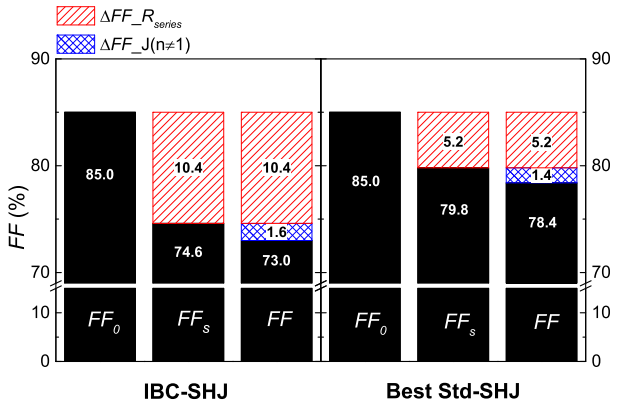

Fig. 5. Charge–carrier transport and recombination influences on solar cell *FF*: Ideal *FF* (FF_0), series-resistance-affected *FF* (FF_s), and measured *FF* (from illuminated *I–V* measurements) of our IBC-SHJ and best Std-SHJ devices [29].

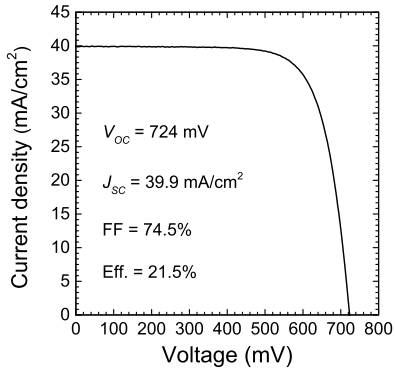

Fig. 6. *I–V* characteristic of the best 9-cm^2 IBC-SHJ device.

transport, as well as carrier recombination processes. Quantitative analysis of such *FF* losses is complex, and carrier-injection-level-dependent effects of these mechanisms can further complicate this type of study. In the following analysis, we calculate *FF* resistance losses using the measured series-resistance ($R_{\rm series}$) and shunt-resistance ($R_{\rm sh}$) values and estimate and compare the amount of *FF* recombination losses in both IBC- and best Std-SHJ devices. Resistance values normalized to the designated cell area are indicated with the superscript N.

The normalized series resistance associated with our IBC-SHJ solar cell, extracted from the comparison of 1-sun *I–V* and dark *I–V* curves [32], equals $R_{\rm series}^{N,\rm IBC} = 2.1\ \Omega{\cdot}{\rm cm}^2$. This value is significantly higher than what we find for our best Std-SHJ solar cell: $R_{\rm series}^{N,\rm FJ} = 1.1\ \Omega{\cdot}{\rm cm}^2$. The *FF* losses associated with these extracted series-resistance values ($\Delta FF\_R_{\rm series}$) can be calculated from the difference between the ideal *FF* (FF_0) and the series-resistance-affected *FF* (FF_s), using the semiempirical expressions reported by Green (see Fig. 5) [33]: $FF_0 = \frac{v_{\rm oc} - \ln(v_{\rm oc}+0.72)}{v_{\rm oc}+1}$ and $FF_{\rm s} = FF_0\,(1 - 1.1r_s) + \frac{r_s^2}{5.4}$. In these expressions, $v_{\rm OC}$ and r_s are defined as $v_{\rm oc} = \frac{V_{\rm oc}}{nKT/q}$ and $r_s = \frac{R_{\rm series}}{V_{\rm oc}/I_{\rm sc}}$, respectively. FF_0 can be regarded as the *FF* of a diode *I–V* curve, of diode ideality factor n, offset by a value equal to the photogenerated current, and intersecting the abscissa $I = 0$ A at a voltage equal to $V_{\rm oc}$. This function scales with increasing $V_{\rm oc}$ values, and for given temperature and n values, it depends only on $V_{\rm oc}$. Practically, for a solar cell with a given $V_{\rm oc}$, FF_0 represents the highest theoretically possible *FF*, assuming only the presence of recombination mechanisms with an ideality factor n, where $R_{\rm series}$ equals zero and $R_{\rm sh}$ is infinitely large. In Table I, we report the values of $\Delta FF\_R_{\rm series}$, calculated assuming $n = 1$. From this, we conclude that the *FF* of our best IBC-SHJ device suffers from increased series-resistance losses. Indeed, in the case of our IBC-SHJ solar cell, $\Delta FF\_R_{\rm series}$ is twice that of the best Std-SHJ solar cell.

The $R_{\rm sh}$ values were extracted from the slope of a linear fit to the dark *I–V* characteristic in the range (0, −100) mV. For the IBC- and best Std-SHJ solar cells, normalized $R_{\rm sh}$ equals, respectively, $R_{\rm sh}^{N,\rm IBC} = 0.5 \times 10^5\ \Omega{\cdot}{\rm cm}^2$ and $R_{\rm sh}^{N,\rm FJ} = 1.7 \times 10^5\ \Omega{\cdot}{\rm cm}^2$. Similar to the case of $\Delta FF\_R_{\rm series}$, we can estimate the magnitude of *FF* losses associated with $R_{\rm sh}$, by taking the difference between FF_s and series- and shunt-resistance-affected *FF* [33]. We find that shunt-related effects on the overall *FF* are negligible for both of our IBC-SHJ and best Std-SHJ solar cells (in either architecture, <0.1% absolute). This underlines the quality of our patterning methods, resulting in no additional shunting of our IBC-SHJ cells.

Following an approach similar to [34], by considering the difference between FF_s and measured *FF* (from illuminated *I–V* measurements), we can estimate the magnitude of *FF* losses due to recombination currents following ideality factors n different from 1: $\Delta FF\_J(n \neq 1) = FF_s - FF$ (see Fig. 5). ΔFF_J $(n \neq 1)$ in the case of our IBC-SHJ device appears to be almost equal to the case of the best Std-SHJ device, demonstrating that *FF* recombination losses in IBC-SHJ cells can be as low as in Std-SHJ devices.

C. Best Interdigitated Back-Contacted Silicon Heterojunction Solar Cell Results and Discussion

The 1-sun *I–V* characteristic of our best 9-cm^2 IBC-SHJ solar cell is given in Fig. 6. This best solar cell belongs to an entire class of devices fabricated with a-Si:H layers, different from the case of the best certified Std-SHJ solar cell, in which the plasma conditions were specifically tuned for improved carrier transport at the two heterocontacts. It shows a conversion efficiency of 21.5%, a $V_{\rm oc}$ of 724 mV, and a $J_{\rm sc}$ of 39.9 mA/cm^2. *FF* reaches a moderate value of 74.5%. Interestingly, the *FF* loss analysis performed in the previous section provides different outcomes in this case. For this device, it results in $R_{\rm series}^{N,\rm IBC}$ $= 1.3\ \Omega{\cdot}{\rm cm}^2$ and $\Delta FF\_R_{\rm series} = 6.6\%$. Thus, series-resistance losses are only slightly higher than for the best Std-SHJ device. However, $\Delta FF\_J(n \neq 1)$ is large in this case, accounting for 3.8% absolute *FF* losses (see Table I). The increased value of $\Delta FF\_J(n \neq 1)$ can be clearly linked with a lack of passivation in the carrier carrier-injection range $<3 \times 10^{15}$ cm^{-3}. By calculating the implied *FF* value from the injection-level-dependent lifetime data of the best IBC-SHJ precursor (as described in [29]), after the deposition of all intrinsic and doped a-Si:H layers, we extract a value that is around 2% lower than for typical Std-SHJ precursors. Importantly, this lack of

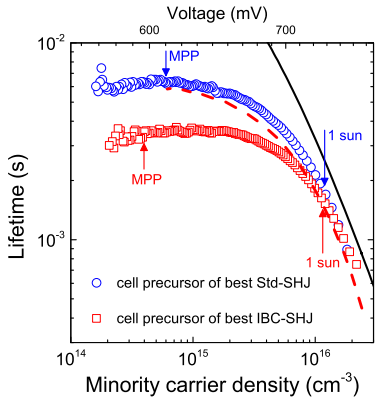

Fig. 7. Minority carrier effective lifetimes of the best IBC- and best Std-SHJ solar cell precursors after deposition of all intrinsic and doped a-Si:H layers (no other contacting layers are present). Implied voltages, calculated according to [36] and assuming a wafer resistivity of 3 Ω·cm ($N_D = 1.4 \times 10^{15}\,\mathrm{cm}^{-3}$), are reported on the top axis. The injection levels corresponding to 1-sun illumination and the MPP of finished devices are marked by solid arrows. The combined Auger and radiative limit is indicated by the solid line [37]. High minority carrier effective lifetime curves were also achieved for IBC-SHJ precursors; the dashed red line shows the lifetime curve associated with the solar cell precursor of the IBC-SHJ device analyzed in Sections III-A and B.

passivation is not intrinsically linked to the IBC-SHJ process flow or device architecture, as we also fabricated IBC-SHJ cell precursors with excellent passivation over the complete injection range (see Fig. 7), yielding implied *FF* values as those of typical Std-SHJ cell precursors. This is the case for the cell precursor of the IBC-SHJ solar cell presented in Sections III-A and B; however, with the type of layers used in this cell, $\Delta FF\_R_{\mathrm{series}}$ was larger, compared with that of the class of IBC-SHJ devices presented in this section, and thus, final cell *FF* values over 74.5% have yet to be achieved. These findings suggest that passivation and carrier transport properties of a-Si:H layer contact stacks are entangled, and their independent optimization is not trivial.

Our IBC-SHJ devices reach conversion efficiencies of over 21%, using the described simple processes. This is on par with the best published back-contacted SHJ devices [10], [11], [35], excluding the outstanding results of Panasonic [8] and Sharp [9], of which precise details about the fabrication complexity are undisclosed.

For the sake of completeness, we briefly remark on the care to be taken when performing the proposed *FF* loss analysis. When very high-quality passivation is achieved, recombination during the solar cell operation is driven mainly by radiative and Auger recombination, with the latter dominant. To account for this in the calculation of the ideal FF_0, the ideality factor should be set, in principle, to $n = 2/3$ [38], yielding an increased ideal FF_0 value. This increases the upper limit for the *FF*, but leaves the conclusions about the relative importance of resistance and recombination losses in our IBC-SHJ devices unchanged. Additionally, in back-contacted solar cells, effects linked to the 2-D character of such devices and to locally different carrier injection levels must not be underestimated. At the back side of these devices, indeed, several interfaces are present, with different recombination behavior, and even current crowding effects toward the heterocontacts can be envisaged. Despite this, in the case of our IBC-SHJ devices, we deal with "well-behaved" diodes with dark *I–V* characteristics that can be easily fitted with a classical two-diode model [39] and for which the described analysis is valid (data not shown).

D. Series-Resistance Components in Interdigitated Back-Contacted Silicon Heterojunction Solar Cells

In the previous sections, we concluded that series-resistance losses are an important limiting factor for the *FF* of IBC-SHJ devices. Here, we analyze in detail the main different components contributing to the device total series resistance. In general, these can be divided into three classes:

1) base resistance (R_{base}) of the wafer;
2) finger (R_{finger}) and busbar (R_{bb}) grid resistances;
3) heterocontact resistances (R_{contact}).

R_{base} is linked to charge–carrier lateral transport in the bulk of the wafer between the two comb electrodes. R_{finger} and R_{bb} are associated with electrical conduction into the TCO/metal back contact; $(R_{\mathrm{finger}})_p$ and $(R_{\mathrm{bb}})_p$ refer to the emitter comb; and $(R_{\mathrm{finger}})_n$ and $(R_{\mathrm{bb}})_n$ refer to the base comb. $(R_{\mathrm{contact}})_p$ and $(R_{\mathrm{contact}})_n$ are linked, respectively, to transport through the emitter heterocontact (n-type c-Si/intrinsic a-Si:H/p-type a-Si:H/TCO) and through the base heterocontact (n-type c-Si/intrinsic a-Si:H/n-type a-Si:H/TCO). Note that both stacks feature several interfaces each possibly affecting R_{contact} and, consequently, R_{series}.

The several orders of magnitude difference between metal and TCO layer resistivity cause the latter to act in principle as a buffer layer for *transverse* carrier extraction. However, as a result of typical TCO resistivity (1–2 × 10^{-3} Ω·cm), TCO thickness (≤100 nm), and TCO/metal specific contact resistivity (<1 × 10^{-3} Ω·cm^2), series-resistance contributions linked with transport through the TCO layer to the metal layer, perpendicular to the wafer, are negligible (<1 × 10^{-2} Ω·cm^2). Due to the difference in metal and TCO layer resistivity, the TCO does not contribute to *lateral* carrier conduction into the back contact. The R_{finger} and R_{bb} values can, thus, be considered as merely metal line resistances. The typical values indicated above are those of the layers employed in our IBC-SHJ devices; TCO resistivity was measured by Hall effect measurements, TCO thickness using a stylus profiler, and TCO/metal specific contact resistivity by means of the transfer length method [40].

The precise derivation of the series-resistance components specific to our IBC-SHJ solar cell design is given in the Appendix. The normalized cell series resistance (R^N_{series}) equals

$$R^N_{\mathrm{series}} = R^N_{\mathrm{base}} + \left(R^N_{\mathrm{finger}} + R^N_{\mathrm{bb}} + R^N_{\mathrm{contact}}\right)_n + \left(R^N_{\mathrm{finger}} + R^N_{\mathrm{bb}} + R^N_{\mathrm{contact}}\right)_p . \quad (1)$$

Based on (1), we now evaluate the magnitude of the different series-resistance components and their associated *FF* losses. For this, we take experimental values from our IBC-SHJ solar cells for the wafer and TCO/metal stack properties, back-contact geometry, and minority carrier injection level at the maximum power point (MPP).

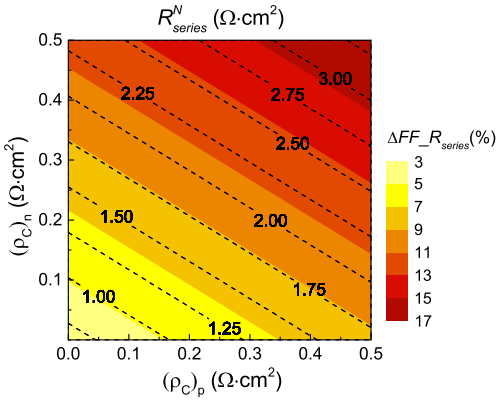

Fig. 8. Normalized series resistance (R^N_{series} $(\Omega \cdot \text{cm}^2)$) of IBC-SHJ devices and associated absolute *FF* loss [$\Delta FF\_R_{\text{series}}$ (%)] as a function of heterocontact specific contact resistivity. Dashed contour lines delimitate regions of R^N_{series} values, whereas the color map is used to represent $\Delta FF\_R_{\text{series}}$ values.

We find that transport losses at the heterocontacts have a preponderant role in the determination of the total device R^N_{series} and the associated $\Delta FF\_R_{\text{series}}$ In a range of specific contact resistivity values 0.1–0.5 Ω·cm^2, for both emitter $((\rho_c)_p)$ and base $((\rho_c)_n)$ heterocontacts, the *FF* loss associated with only the contact resistance component goes from a minimum of 2.7% absolute to a value of 13.8% absolute, which are indeed significant losses. The range 0.1–0.5 Ω·cm^2 covers most of the values reported in the literature for the specific contact resistivity of the heterocontacts [10], [41], [42]. On the other hand, the *FF* loss associated with lateral conduction in the base accounts for 1.6% absolute, and the overall *FF* loss associated with the different grid resistance components is 1.7% absolute. In Fig. 8, we give calculated values of R^N_{series}, and of the associated total $\Delta FF\_R_{\text{series}}$, as a function of the specific contact resistivity values of both stacks. Fig. 8 shows how contact resistance can have an important detrimental influence on the final device *FF* value.

FF losses associated with heterocontact transport properties can be at least partially ascribed to the TCO/a-Si:H interface [10], [43]–[46]. Our experimental work with IBC-SHJ confirms the importance of this interface with respect to series-resistance losses; changes in the TCO layer composition have shown a relevant impact on total series resistance and *FF* of final devices (data not shown), as have changes in the deposition conditions of the doped a-Si:H layers. However, characterization of the detailed heterocontact transport properties is complex, and we believe that additional efforts in this regard are needed. Increased insights into the transport mechanisms at the heterocontacts would help further optimization.

E. Interdigitated Back-Contacted Silicon Heterojunction Fill Factor Limiting Factors

Basic modeling of the different series-resistance components in IBC-SHJ devices and analysis of *FF* losses in IBC-SHJ devices demonstrate that series resistance can limit final cell *FF* values.

For IBC devices, a front-diffused layer may help to achieve high *FF* either by improving front-surface recombination behavior [47] or enhancing lateral transport and reducing R_{base} component [48]. However, the latter depends on the wafer injection level under solar cell working conditions. Assuming typical passivation quality of a-Si:H films (high injection level under solar cell working conditions, i.e., MPP) and a suitable pitch for the back-contact geometry, we think that such front-diffused layers can be avoided in IBC-SHJ devices without incurring large lateral transport losses.

The level of transport optimization at the two heterocontacts in IBC-SHJ devices assumes an increased relevance compared with typical Std-SHJ devices. This augmented relevance comes from a minor degree of freedom in the optimization of the two contact stacks and an overall reduced contact area. In the proposed processing sequence, TCO is deposited by a unique deposition process, and thus, it cannot be optimized independently for each single heterocontact, unless an increased amount of processing steps can be accepted. The same occurs for the back intrinsic a-Si:H layer. Next, the overall area occupied by the heterocontacts is reduced to less than half with respect to any typical two-side-contacted SHJ solar cell. This significantly increases the current densities through the heterocontacts; for our back-contact geometry, current densities of 80 mA/cm^2 and of 130 mA/cm^2, for the emitter and base heterocontacts, respectively, must be collected, compared with about 40 mA/cm^2 for typical Std-SHJ cells. The type of a-Si:H layers that led to our best IBC-SHJ device demonstrates that these *FF* transport losses can be minimized. However, this was achieved at the expense of increased *FF* recombination losses. Efforts to resolve these problems will also benefit Std-SHJ devices.

These conclusions on the importance of electrical contact optimization are limited to back-contacted SHJ devices; in the case of typical back-contacted homojunction devices, specific contact resistivity values are significantly lower and the contact area must be limited to openings through dielectric passivation layers [49]–[54] to allow for high-V_{oc} devices. Interestingly, in both cases, we eventually face a tradeoff between recombination and transport losses.

IV. Conclusion

Back-contacted SHJ devices, using interdigitated back contacts, with conversion efficiencies of up to 21.5% have been fabricated by a simple processing sequence and size-scalable techniques. The added complexity typically associated with IBC process flows has been minimized. *In situ* masking of a-Si:H layers has been demonstrated to be a viable patterning method for high-efficiency devices. J_{sc} values have been shown to benefit from the back-contacted architecture, and V_{oc} values have been shown not to suffer from the additional processing required by the proposed fabrication methodology. Moderate *FF* values remain the main limiting factor for higher device efficiencies. *FF* losses related to transport and recombination currents have been studied in our IBC-SHJ devices and compared with our best Std-SHJ device. Based on this analysis, higher device *FF* and efficiencies are possible, using the proposed processing solution,

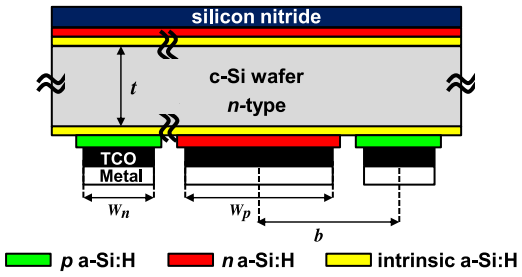

Fig. 9. Geometry of the back contact. Side view.

via further optimization of transport at the two heterocontacts and high-quality a-Si:H passivation layers.

APPENDIX

The interdigitated back contact consists of two combs, each with n fingers of length a and width w, which half-pitch is indicated with the parameter b. In the following text, when present, subscripts n and p specify, respectively, the n-type and the p-type comb (see Fig. 9). The designated cell area [see (3)–(5)] is indicated with the parameter A_d.

Equation (2) for the normalized series-resistance base component is taken from [55] and reformulated according to our specific device architecture. For substrate, we assume an n-type wafer of thickness t, resistivity ρ_w, and with a donor-dopant density equal to N_D. The solar cell injection level at MPP (Δp) is calculated from V_{mpp} of the resistance-free *I–V* curve, measured by suns-V_{oc}, according to [36]

$$R^N_{\mathrm{base}} \cong \frac{\rho_w N_D}{(N_D+\Delta p)}\left(\frac{b\cdot(b-w_n/2-w_p/2)}{t}+\frac{b\cdot w_p/2}{3t}\right). \tag{2}$$

The expressions for the normalized metal grid series-resistance component [see (3) and (4)] of each comb are derived, as reported in [56]. The TCO/metal stack is a unique conduction medium, whose sheet resistance equals the measured value $R^{\mathrm{metal/TCO}}_{\mathrm{sheet}} = 0.02\Omega/\square$. The prefactor in (4) accounts for three current-extraction points along each busbar (of width $w\prime$), as in our measurement setup

$$R^N_{\mathrm{finger}} = \frac{4}{3}a^3b^2n\left(\frac{R^{\mathrm{metal/TCO}}_{\mathrm{sheet}}}{w}\right)\cdot\frac{1}{A_d} \tag{3}$$

$$R^N_{\mathrm{bb}} = \frac{2}{27}a^2n^3b^3\left(\frac{R^{\mathrm{metal/TCO}}_{\mathrm{sheet}}}{w'}\right)\cdot\frac{1}{A_d}. \tag{4}$$

The normalized resistance components associated with the heterocontacts are calculated according to (5). Modifying (5) to account for carrier collection below the contacts over a region wide as the transfer length $L_{t(c)}$, the conclusions from Section III-D remain unchanged

$$\left(R^N_{\mathrm{contact}}\right)_p = \frac{(\rho_C)_p}{w_p n a}\cdot A_d \quad \left(R^N_{\mathrm{contact}}\right)_n = \frac{(\rho_C)_n}{w_n n a}\cdot A_d. \tag{5}$$

ACKNOWLEDGMENT

The authors would like to thank Roth & Rau Research for scientific and financial partnership and wafer preparation; CSEM for scientific support and wafer preparation; J. Hermans and Roth & Rau B.V. for the support in inkjet printing; N. Holm for precious help in PECVD layer deposition; and P. Löper and L. Barraud for discussion on solar cell *FF* losses.

REFERENCES

[1] S. De Wolf, A. Descoeudres, Z. C. Holman, and C. Ballif, "High-efficiency silicon heterojunction solar cells: A review," *Green*, vol. 2, pp. 7–24, Feb. 2012.
[2] M. Taguchi, A. Yano, S. Tohoda, K. Matsuyama, Y. Nakamura, T. Nishiwaki, K. Fujita, and E. Maruyama, "24.7% Record efficiency HIT solar cell on thin silicon wafer," *IEEE J. Photovoltaics*, vol. 4, no. 1, pp. 96–99, Jan. 2014.
[3] E. Demesmaeker, J. Symons, J. Nijs, and R. Mertens, "The influence of surface recombination on the limiting efficiency and optimum thickness of silicon solar cells," in *Proc. 10th Eur. Photovoltaic Sol. Energy Conf.*, Lisbon, Portugal, 1991, pp. 66–69.
[4] J. Zhao, A. Wang, M. A. Green, and F. Ferrazza, "19.8% efficient "honeycomb" textured multicrystalline and 24.4% monocrystalline silicon solar cells," *Appl. Phys. Lett.*, vol. 73, no. 14, pp. 1991–1993, Oct. 1998.
[5] P. J. Cousins, D. D. Smith, L. Hsin-Chiao, J. Manning, T. D. Dennis, A. Waldhauer, K. E. Wilson, G. Harley, and W. P. Mulligan, "Generation 3: Improved performance at lower cost," in *Proc. IEEE 35th Photovoltaic Spec. Conf.*, Honolulu, HI, USA, 2010, pp. 275–278.
[6] Z. C. Holman, A. Descoeudres, L. Barraud, F. Z. Fernandez, J. P. Seif, S. De Wolf, and C. Ballif, "Current losses at the front of silicon heterojunction solar cells," *IEEE J. Photovoltaics*, vol. 2, no. 1, pp. 7–15, Jan. 2012.
[7] Z. C. Holman, A. Descoeudres, S. De Wolf, and C. Ballif, "Record infrared internal quantum efficiency in silicon heterojunction solar cells with dielectric/metal rear reflectors," *IEEE J. Photovoltaics*, vol. 3, no. 4, pp. 1243–1249, Oct. 2013.
[8] "Panasonic HIT® solar cell achieves world's highest energy conversion efficiency of 25.6% at research level," Public Relations Development Office, Panasonic Corp., Osaka , Japan, Apr. 2014.
[9] K. K. N. Koide, T. Sakai, T. Kuniyoshi, H. Katayama, N. Asano, T. Hieda, and J. Nakamura, "High efficient crystalline Si solar cells with rear heterojunction emitter and antireflective passivation layer," presented at the 23rd Photovoltaic Specialist Conf., Taipei, Taiwan, 2013.
[10] S.-Y. Lee, H. Choi, H. Li, K. Ji, S. Nam, J. Choi, S.-W. Ahn, H.-M. Lee, and B. Park, "Analysis of a-Si:H/TCO contact resistance for the Si heterojunction back-contact solar cell," *Sol. Energy Mater. Sol. Cells*, vol. 120, pp. 412–416, Jan. 2014.
[11] N. Mingirulli, J. Haschke, R. Gogolin, R. Ferre, T. F. Schulze, J. Dusterhoft, N. P. Harder, L. Korte, R. Brendel, and B. Rech, "Efficient interdigitated back-contacted silicon heterojunction solar cells," *Phys. Status Solidi-Rapid Res. Lett.*, vol. 5, no. 4, pp. 159–161, Apr. 2011.
[12] S. De Vecchi, T. Desrues, F. Souche, D. Muñoz, and M. Lemiti, "Laser assisted patterning of hydrogenated amorphous silicon for interdigitated back contact silicon heterojunction solar cell," presented at the Laser Mater. Process. Sol. Energy, San Diego, CA, USA, 2012.
[13] Z. R. Chowdhury, D. Stepanov, D. Yeghikyan, and N. P. Kherani, "Excellent low temperature passivation scheme with reduced optical absorption for back amorphous-crystalline silicon heterojunction (BACH) photovoltaic device," in *Proc. 38th IEEE Photovoltaic Spec. Conf.*, Austin, TX, USA, 2012, pp. 001026–001028.
[14] U. Das, H. Jianbo, S. Zhan, Z. Lulu, C. Thompson, R. Birkmire, and S. Hegedus, "Sensitivity of surface passivation and interface quality in IBC-SHJ solar cells to patterning process," in *Proc. IEEE 39th Photovoltaic Spec. Conf.*, Tampa, FL, USA, 2013, pp. 1224–1227.
[15] M. Tucci, L. Serenelli, E. Salza, L. Pirozzi, G. de Cesare, D. Caputo, M. Ceccarelli, P. Martufi, S. De Iuliis, and L. J. Geerligs, "Back enhanced heterostructure with interdigitated contact—BEHIND—solar cell," in *Proc. Conf. Optoelectro. Microelectron. Mater. Devices*, Sydney, Australia, 2008, pp. 242–245.
[16] Y.-Y. Chen, L. Korte, C. Leendertz, J. Haschke, J.-Y. Gan, and D.-C. Wu, "Simulation of contact schemes for silicon heterostructure rear contact solar cells," *Energy Procedia*, vol. 38, pp. 677–683, Mar. 2013.

[17] S. De Vecchi, T. Desrues, F. Souche, D. Muñoz, P. J. Ribeyron, and M. Lemiti, "Point contact technology for silicon heterojunction solar cells," *Energy Procedia*, vol. 27, pp. 549–554, Apr. 2012.

[18] R. Stangl, J. Haschke, M. Bivour, L. Korte, M. Schmidt, K. Lips, and B. Rech, "Planar rear emitter back contact silicon heterojunction solar cells," *Sol. Energy Mater. Sol. Cells*, vol. 93, no. 10, pp. 1900–1903, Oct. 2009.

[19] J. Haschke, N. Mingirulli, and B. Rech, "Progress in point contacted rear silicon heterojunction solar cells," in *Proc. 2nd Int. Conf. Crystalline Silicon Photovoltaics*, Amsterdam, The Netherlands, 2012, pp. 116–121.

[20] M. Tucci, L. Serenelli, E. Salza, S. De Iuliis, L. J. Geerligs, G. de Cesare, D. Caputo, and M. Ceccarelli, "Novel scheme of amorphous/crystalline silicon heterojunction solar cell," in *Proc. 22nd Eur. Photovoltaic Sol. Energy Conf.*, Milan, Italy, 2007, pp. 1600–1603.

[21] T. Desrues, P.-J. Ribeyron, A. Vandeneynde, A.-S. Ozanne, F. Souche, Y. Veschetti, A. Bettinelli, P. Roca i Cabarrocas, M. Labrune, D. Diouf, J.P. Kleider, and M. Lemiti, "New process integration for interdigitated back contact (IBC) a-Si:H/c-Si heterojunction solar cells," in *Proc. 23rd Eur. Photovoltaic Sol. Energy Conf. Exhib.*, Valencia, Spain, 2008, pp. 1673–1676.

[22] M. Scherff, "Novel method for preparation of interdigitated back contacted a-Si:H/c-Si heterojunction solar cells," in *Proc. 26th Eur. Photovoltaic Sol. Energy Conf. Exhib.*, Hamburg, Germany, 2011, pp. 2125–2129.

[23] K. Ohdaira, K. Koyama, K. Sugita, and H. Matsumura, "A novel technique to fabricate back contact HIT solar cells by simple hard mask process without photolithography," in *Proc. 21st Eur. Photovoltaic Sol. Energy Conf. Exhib.*, Dresden, Germany, 2006, pp. 1716–2006.

[24] A. Descoeudres, L. Barraud, S. De Wolf, B. Strahm, D. Lachenal, C. Guerin, Z. C. Holman, F. Zicarelli, B. Demaurex, J. Seif, J. Holovsky, and C. Ballif, "Improved amorphous/crystalline silicon interface passivation by hydrogen plasma treatment," *Appl. Phys. Lett.*, vol. 99, no. 12, pp. 123506-1–123506-3, Sep. 2011.

[25] S. De Wolf and M. Kondo, "Nature of doped a-Si:H/c-Si interface recombination," *J. Appl. Phys.*, vol. 105, no. 10, pp. 103707-1–103707-6, May 2009.

[26] L. L. Zhang, B. Shu, R. Birkmire, S. Hegedus, and U. Das, "Impact of back surface patterning process on FF in IBC-SHJ," in *Proc. IEEE 38th Photovoltaic Spec. Conf.*, Austin, TX, USA, 2012, pp. 1177–1181.

[27] N. Mingirulli, R. Keding, J. Specht, A. Fallisch, D. Stuwe, and D. Biro, "Hot-melt inkjet as masking technology for back-contacted cells,," in *Proc. IEEE 34th Photovoltaic Spec. Conf.*, Philadelphia, PA, USA, 2009, pp. 001064–001068.

[28] T. Desrues, S. De Vecchi, F. Souche, D. Diouf, D. Muñoz, M. Gueunier-Farret, J.-P. Kleider, and J.-P. Ribeyron, "Development of interdigitated back contact silicon heterojunction (IBC Si-HJ) solar cells," *Energy Procedia*, vol. 8, pp. 294–300, Apr. 2011.

[29] A. Descoeudres, Z. C. Holman, L. Barraud, S. Morel, S. De Wolf, and C. Ballif, ">21% Efficient silicon heterojunction solar cells on n- and p-type wafers compared," *IEEE J. Photovoltaics*, vol. 3, no. 1, pp. 83–89, Jan. 2013.

[30] M. Hermle, F. Granek, O. Schultz-Wittmann, and S.W. Glunz, "Shading effects in back-junction back-contacted silicon solar cells,," in *Proc. IEEE 33rd Photovoltaic Spec. Conf.*, San Diego, CA, USA, 2008, pp. 1–4.

[31] C. Reichel, F. Granek, M. Hermle, and S. W. Glunz, "Investigation of electrical shading effects in back-contacted back-junction silicon solar cells using the two-dimensional charge collection probability and the reciprocity theorem," *J. Appl. Phys.*, vol. 109, no. 2, pp. 024507-1–024507-12, Jan. 2011.

[32] D. Pysch, A. Mette, and S. W. Glunz, "A review and comparison of different methods to determine the series resistance of solar cells," *Sol. Energy Mater. Sol. Cells*, vol. 91, no. 18, pp. 1698–1706, Nov. 2007.

[33] M. A. Green, "Accuracy of analytical expressions for solar cell fill factors," *Sol. Cells*, vol. 7, no. 3, pp. 337–340, Dec. 1982.

[34] A. Khanna, T. Mueller, R .A. Stangl, B. Hoex, P. K. Basu, and A. G. Aberle, "A fill factor loss analysis method for silicon wafer solar cells," *IEEE J. Photovoltaics*, vol. 3, no. 4, pp. 1170–1177, Oct. 2013.

[35] T. Desrues, S. De Vecchi, F. Souche, D. Munoz, and P. J. Ribeyron, "SLASH concept: A novel approach for simplified interdigitated back contact solar cells fabrication," in *Proc. IEEE 38th Photovoltaic Spec. Conf.*, New York, NY, USA, 2012, pp. 1602–1605.

[36] R. A. Sinton and A. Cuevas, "Contactless determination of current–voltage characteristics and minority-carrier lifetimes in semiconductors from quasi-steady-state photoconductance data," *Appl. Phys. Lett.*, vol. 69, no. 17, pp. 2510–2512, Oct. 1996.

[37] A. Richter, S. W. Glunz, F. Werner, J. Schmidt, and A. Cuevas, "Improved quantitative description of Auger recombination in crystalline silicon," *Phys. Rev. B*, vol. 86, no. 16, pp. 165202-1–165202-14, Oct. 2012.

[38] R. N. Hall, "Silicon photovoltaic cells," *Solid-State Electron.*, vol. 24, no. 7, pp. 595–616, Jul. 1981.

[39] M. Wolf and H. Rauschenbach, "Series resistance effects on solar cell measurements," *Adv. Energy Convers.*, vol. 3, no. 2, pp. 455–479, Apr. 1963.

[40] H. H. Berger, "Models for contacts to planar devices," *Solid-State Electron.*, vol. 15, no. 2, pp. 145–158, Feb. 1972.

[41] J. Haschke, Y.-Y. Chen, R. Gogolin, M. Mews, N. Mingirulli, L. Korte, and B. Rech, "Approach for a simplified fabrication process for IBC-SHJ solar cells with high fill factors," *Energy Procedia*, vol. 38, pp. 732–736, Mar. 2013.

[42] R. Gogolin, M. Turcu, R. Ferré, R. Brendel, N.-P. Harder, and J. Schmidt, "730 mV bifacial screen printed a-Si:H/c-Si heterojunction solar cells: Open-circuit voltage and fill factor effect from a-Si:H layer thickness and front metellization," in *Proc. 28th Eur. Photovoltaic Sol. Energy Conf. Exhib.*, Paris, France, 2013, pp. 1039–1042.

[43] R. Rößler, C. Leendertz, L. Korte, N. Mingirulli, and B. Rech, "Impact of the transparent conductive oxide work function on injection-dependent a-Si:H/c-Si band bending and solar cell parameters," *J. Appl. Phys.*, vol. 113, no. 14, pp. 144513-1–144513-8, Apr. 2013.

[44] S. Lee, S. J. Tark, C. S. Kim, D. Y. Jeong, J. C. Lee, W. M. Kim, and D. Kim, "Influence of front contact work function on silicon heterojunction solar cell performance," *Current Appl. Phys.*, vol. 13, no. 5, pp. 836–840, Jul. 2013.

[45] R. Lachaume, W. Favre, P. Scheiblin, X. Garros, N. Nguyen, J. Coignus, D. Munoz, and G. Reimbold, "Influence of a-Si:H/ITO interface properties on performance of heterojunction solar cells," *Energy Procedia*, vol. 38, pp. 770–776, Mar. 2013.

[46] M. Bivour, S. Schröer, and M. Hermle, "Numerical analysis of electrical TCO / a-Si:H(p) contact properties for silicon heterojunction solar cells," *Energy Procedia*, vol. 38, pp. 658–669, Mar. 2013.

[47] T. Ohrdes, U. Römer, Y. Larionova, R. Peibst, P. P. Altermatt, and N.-P. Harder, "High fill-factors of back-junction solar cells without front surface field diffusion," in *Proc. 27th Eur. Photovoltaic Sol. Energy Conf. Exhib.*, Frankfurt, Germany, 2012, pp. 866–869.

[48] F. Granek, M. Hermle, D. M. Huljić, O. Schultz-Wittmann, and S. W. Glunz, "Enhanced lateral current transport via the front N+ diffused layer of n-type high-efficiency back-junction back-contact silicon solar cells," *Progr. Photovoltaics, Res. Appl.*, vol. 17, no. 1, pp. 47–56, Jan. 2009.

[49] K. C. Fong, K. Teng, K .R. McIntosh, A. W. Blakers, E. Franklin, S. Z. Ngwe, and A. Fell, "Optimisation of N+ diffusion and contact size of IBC solar cells," in *Proc. 28th Eur. Photovoltaic Sol. Energy Conf. Exhib.*, Paris, France, 2013, pp. 851–855.

[50] N. E. Posthuma, J. Robbelein, S. Singh, M. Debucquoy, K. Wostyn, B. J. Pawlak, X. Loozen, J. Fernández, P. J. Verlinden, and J. Poortmans, "Development and analysis of small area high efficiency interdigitated back contact silicon solar cells," in *Proc. 27th Eur. Photovoltaic Sol. Energy Conf. Exhib.*, Frankfurt, Germany, 2012, pp. 571–575.

[51] R. Peibst, N.-P. Harder, A. Merkle, T. Neubert, S. Kirstein, J. Schmidt, F. Dross, P.A. Basore, and R. Brendel, "High-efficiency RISE-IBC solar cells: Influence of rear side-passivation on pn-junction meander recombination," in *Proc. 28th Eur. Photovoltaic Sol. Energy Conf. Exhib.*, Paris, France, 2013, pp. 971–975.

[52] R. R. King, R. A. Sinton, and R. M. Swanson, "Doped surfaces in one sun, point-contact solar cells," *Appl. Phys. Lett.*, vol. 54, no. 15, pp. 1460–1462, Apr. 1989.

[53] C. Gong, S. Singh, J. Robbelein, N. Posthuma, E. Van Kerschaver, J. Poortmans, and R. Mertens, "High efficient n-type back-junction back-contact silicon solar cells with screen-printed Al-alloyed emitter and effective emitter passivation study," *Progr. Photovoltaics, Res. Appl.*, vol. 19, no. 7, pp. 781–786, Nov. 2011.

[54] C. Reichel, F. Granek, M. Hermle, and S. W. Glunz, "Back-contacted back-junction n-type silicon solar cells featuring an insulating thin film for decoupling charge carrier collection and metallization geometry," *Progr. Photovoltaics, Res. Appl.*, vol. 21, no. 5, pp. 1063–1076, Aug. 2013.

[55] P. J. Verlinden, M. Aleman, N. Posthuma, J. Fernandez, B. Pawlak, J. Robbelein, M. Debucquoy, K. Van Wichelen, and J. Poortmans, "Simple power-loss analysis method for high-efficiency Interdigitated Back Contact (IBC) silicon solar cells," *Sol. Energy Mater. Sol. Cells*, vol. 106, pp. 37–41, Nov. 2012.

[56] D. L. Meier and D. K. Schroder, "Contact resistance: Its measurement and relative importance to power loss in a solar cell," *IEEE Trans. Electron. Devices*, vol. ED-31, no. 5, pp. 647–653, May 1984.

Andrea Tomasi received the Master's degree in physics from the University of Bologna, Bologna, Italy, in 2007 with a thesis on the electrical characterization of nc-Si:H thin films for applications in photovoltaics. Since 2012, he has been working toward the Ph.D. degree on the development of innovative high-efficiency silicon heterojunction solar cell architectures with the Photovoltaics and Thin-Film Electronics Laboratory, École Polytechnique Fédérale de Lausanne, Neuchâtel, Switzerland.

From 2007 to 2011, he was with Xgroup, Padua, Italy, where he was in charge of the ramp-up of few production lines of multicristalline silicon solar cells and of the technological development of the solar cell production process.

Bertrand Paviet-Salomon was born in Lyon, France, in 1986. He received the M.Sc. degree in 2009 and the Engineer Diploma degree in theoretical and applied optics from the Institut d'Optique, Paris, France. From 2009 to 2012, he was a Ph.D. student with the French National Institute for Solar Energy, Le-Bourget-du-Lac, France, working on laser processes for crystalline silicon solar cells. He received the Ph.D. degree in electronics and photonics from the University of Strasbourg, Strasbourg, France, in 2012.

In 2012, he joined the Photovoltaics and Thin-Film Electronics Laboratory, École Polytechnique Fédérale de Lausanne, Neuchâtel, Switzerland, as a Postdoctoral Researcher, where he currently develops high-efficiency back-contacted silicon heterojunction solar cells.

Damien Lachenal received the Ph.D. degree in semiconductor physics from the University of Toulon, Toulon, France, in 2007.

He then joined Roth & Rau, Neuchâtel, Switzerland, to start the development of the silicon heterojunction technology as a Development Engineer, where since 2011, he has been a Team Leader of the PECVD group and leads the IBC-SHJ project. His research interests include wet chemistry, PECVD/PVD layer deposition, structuring techniques, cell characterization, and technology transfer from R&D to mass production tools.

Silvia Martin de Nicolas received the M.Sc. and Industrial Engineering degrees from the Universitat Politècnica de Catalunya, Barcelona, Spain, focusing on renewable energy engineering in 2009, and the Ph.D. degree in physics from Université Paris XI, Paris, France, in 2012.

From 2009 to 2012, she was with the French National Institute for Solar Energy (CEA-INES), Le-Bourget-du-Lac, France, where she carried out Ph.D. research on silicon heterojunction technology. In 2013, she joined the Photovoltaics and Thin-Film Electronics Laboratory, École Polytechnique Fédérale de Lausanne, Neuchâtel, Switzerland, as a Postdoctoral Researcher, where she is working on high-efficiency silicon heterojunction devices.

Antoine Descoeudres received the M.Sc. and Ph.D. degrees in physics from École Polytechnique Fédérale de Lausanne, Neuchâtel, Switzerland, in 2001 and 2006, respectively.

From 2007 to 2009, he was a Postdoctoral Researcher with CERN, Geneva, Switzerland, working on vacuum breakdowns for the development of high-gradient accelerating cavities. From 2009 to 2013, he was a Postdoctoral Researcher with the Photovoltaics and Thin-Film Electronics Laboratory, École Polytechnique Fédérale de Lausanne, working on the development of silicon heterojunction solar cells. In 2013, he joined the PV-Center, CSEM, Neuchâtel. His current research interests include thin-film deposition with plasma-enhanced chemical vapor deposition and plasma diagnostics for the development of high-efficiency silicon heterojunction solar cells.

Jonas Geissbühler was born in Switzerland in 1988. He received the Bachelor's degree in micro- and nanosciences from the University of Neuchâtel, Neuchâtel, Switzerland. He then studied microengineering with the Ecole Polytechnique Fédérale de Lausanne, Neuchâtel, where he then received the Master's degree, writing his master thesis on the fabrication and characterization of silicon nanowires ion sensitive field-effect transistors, in 2011. Since 2011, he has been working toward the Ph.D. degree with the Photovoltaic and Thin-Film Laboratory, Ecole Polytechnique Fédérale de Lausanne.

His research interests include the fabrication and demonstration of new silicon heterojunction devices using advanced microfabrication techniques.

Stefaan De Wolf received the Ph.D. degree from the Catholic University of Leuven, Leuven, Belgium, while he was with Interuniversity Microelectronics, Leuven, focusing on crystalline silicon solar cells.

From 2005 to 2008, he was with the National Institute of Advanced Industrial Science and Technology, Tsukuba, Japan, focusing on silicon heterojunction devices. In 2008, he joined the Photovoltaics and Thin-Film Electronics Laboratory, Ecole Polytechnique Fédérale de Lausanne, Neuchâtel, Switzerland, as a Team Leader for activities on such solar cells.

Christophe Ballif received the Graduate degree in physics and the Ph.D. degree from the Ecole Polytechnique Fédérale de Lausanne (EPFL), Lausanne, Switzerland, in 1994 and 1998, respectively, focusing on novel photovoltaic materials.

He was a Postdoctoral Researcher with National Renewable Energy Laboratory, Golden, CO, USA, where he was involved in compound semiconductor solar cells (CIGS and CdTe). He then joined the Fraunhofer Institute for Solar Energy Systems, Freiburg, Germany, where he was involved in crystalline silicon photovoltaics (monocrystalline and multicrystalline) until 2003. He then joined the Swiss Federal Laboratories for Materials Testing and Research, Thun, Switzerland, before becoming a Full Professor and Chair with the Institute of Microengineering, University of Neuchâtel, Neuchâtel, Switzerland, in 2004. In 2009, the Institute was transferred to EPFL. He is the Director of the Photovoltaics and Thin-Film Electronics Laboratory within the Institute, as well as of the CSEM PV-Center. His research interests include thin-film solar cells, high-efficiency heterojunction crystalline cells, and module technology contributing to technology transfer and industrialization of novel devices.